Novel lncRNA Erbb4-IR Promotes Diabetic Kidney Injury in *db/db* Mice by Targeting miR-29b

Si F. Sun,[1,2] Patrick M.K. Tang,[1,3] Min Feng,[1,4] Jun Xiao,[1] Xiao R. Huang,[1] Ping Li,[2] Ronald C.W. Ma,[1] and Hui Y. Lan[1]

Diabetes 2018;67:731–744 | https://doi.org/10.2337/db17-0816

Transforming growth factor-β/Smad signaling plays an important role in diabetic nephropathy. The current study identified a novel Smad3-dependent long noncoding RNA (lncRNA) Erbb4-IR in the development of type 2 diabetic nephropathy (T2DN) in *db/db* mice. We found that Erbb4-IR was highly expressed in T2DN of *db/db* mice and specifically induced by advanced glycosylation end products (AGEs) via a Smad3-dependent mechanism. The functional role of Erbb4-IR in T2DN was revealed by kidney-specific silencing of Erbb4-IR to protect against the development of T2DN, such as elevated microalbuminuria, serum creatinine, and progressive renal fibrosis in *db/db* mice, and to block AGE-induced collagen I and IV expression in mouse mesangial cells (mMCs) and mouse tubular epithelial cells (mTECs). Mechanistically, we identified that the Erbb4-IR–microRNA (miR)-29b axis was a key mechanism of T2DN because Erbb4-IR was able to bind the 3′ untranslated region of miR-29b genomic sequence to suppress miR-29b expression at transcriptional level. In contrast, silencing of renal Erbb4-IR increased miR-29b and therefore protected the kidney from progressive renal injury in *db/db* mice and prevented mTECs and mMCs from AGE-induced loss of miR-29b and fibrotic response in vitro. Collectively, we identify that Erbb4-IR is a Smad3-dependent lncRNA that promotes renal fibrosis in T2DN by suppressing miR-29b. Targeting Erbb4-IR may represent a novel therapy for T2DN.

Increasing evidence showed that noncoding RNAs (ncRNAs) play a critical role in a variety of diseases (1). Long ncRNAs (lncRNAs) are defined as a class of >200 nucleotides without protein-coding activity. As lncRNAs are tissue and cell-type specific (1), they have emerged as a new era of gene therapy. Recent studies indicated that lncRNAs are involved in a variety of diseases, such as cancer (2,3), cardiovascular diseases (4,5), and autoimmune diseases (6). In the past decades, many disease-associated ncRNAs have been identified and reported as therapeutic targets for kidney diseases (7–9). However, the expression profile and functions of lncRNAs in diabetic kidney injury remain largely unexplored.

The incidence of diabetic kidney diseases is still increasing continuously worldwide, eventually leading to end-stage renal disease (10). Although a number of studies reported the critical role of microRNAs (miRNAs) in the progression of diabetic nephropathy (DN) (11,12), the applications and potential mechanisms of these miRNAs remain unclear (13). It is well documented that transforming growth factor-β (TGF-β)/Smad signaling is an important pathway leading to renal fibrosis in the diabetic kidney (14). Advanced glycation end products (AGEs) could activate TGF-β/Smad signaling and mediate diabetic scarring directly in TGF-β–dependent and –independent manners (15,16). Recently, two lncRNAs, Tug1 and CHOP, have been identified to promote diabetic kidney diseases in mitochondria- and endoplasmic reticulum–dependent mechanisms, respectively (17,18). However, there is still limited understanding of how lncRNAs regulate the TGF-β/Smad signaling in DN.

We previously identified a number of Smad3-dependent lncRNAs in mice with kidney disease by RNA-sequencing analysis (19,20), in which a novel lncRNA Erbb4-IR (np_5318)

[1]Department of Medicine and Therapeutics, Li Ka Shing Institute of Health Sciences, CUHK-Shenzhen Research Institute, The Chinese University of Hong Kong, Hong Kong SAR, China
[2]Institute of Clinical Medical Sciences, China-Japan Friendship Hospital, Beijing, China
[3]Department of Anatomical and Cellular Pathology, The Chinese University of Hong Kong, Hong Kong SAR, China
[4]Department of Nephrology, Sun Yat-Sen Memorial Hospital, Sun Yat-Sen University, Guangzhou, China
Corresponding author: Hui Y. Lan, hylan@cuhk.edu.hk.

Received 11 July 2017 and accepted 30 November 2017.
This article contains Supplementary Data online at http://diabetes.diabetesjournals.org/lookup/suppl/doi:10.2337/db17-0816/-/DC1.

S.F.S. and P.M.K.T. equally contributed to this work.

See accompanying article, p. 552.

was highly upregulated in the kidney of mice subjected to unilateral ureteral occlusion, but was largely suppressed in mice lacking Smad3 (21). Erbb4-IR is located within the intron region between the first and second exons of Erbb4 gene on chromosome 1 of the mouse genome. We then amplified its full length by rapid amplification of cDNA ends. Chromatin immunoprecipitation clearly demonstrated that Smad3 protein directly binds on the promoter region of Erbb4-IR (21), indicating that Erbb4-IR is a direct Smad3 target gene. In the present work, we explored the pathogenic role of this novel Smad3-dependent lncRNA in type 2 diabetic nephropathy (T2DN). Expression of Erbb4-IR was largely increased and associated with the progression of DN in *db/db* mice. Expression of Erbb4-IR was specifically triggered by AGEs but not high glucose in cultured mouse tubular epithelial cells (mTECs) and mouse mesangial cells (mMCs) and was tightly regulated by a Smad3-dependent mechanism in vitro and in vivo. Importantly, we also found that kidney-specific targeting Erbb4-IR protected *db/db* mice from the development of diabetic kidney injury via a mechanism associated with increasing miR-29b expression under diabetic conditions in vivo and in vitro. Thus, Erbb4-IR may represent a potential therapeutic target for DN.

RESEARCH DESIGN AND METHODS

Animal Model

To detect whether Erbb4-IR expression is Smad3 dependent in *db/db* mice, Smad3-knockout (KO) *db/db* mice were constructed by crossing heterozygous *db/m* with heterozygous Smad3$^{+/-}$ (both from C57BL6 background). We used PCR to genotype the *db* and Smad3 alleles of the first generation of offspring (F1), subsequently identified male and female double-heterozygous mice, and then used them to breed the second generation of offspring (F2). In this study, we examined Erbb4-IR on Smad3 wild-type (WT) *db/m*, Smad3-WT *db/db*, Smad3-KO *db/m*, and Smad3-KO *db/db* mice.

For functional study, male *db/db* mice and their normal littermates (*db/m*) at the age of 4 weeks were purchased from Laboratory Animal Services Centre at The Chinese University of Hong Kong. Groups of eight mice were used: *1*) groups of *db/m* or *db/db* mice were sacrificed at the age of 12 weeks as basic level control; and *2*) groups of *db/m* or *db/db* mice were treated with pSuper.puro vector as negative control (NC) or vector containing short hairpin RNA (shRNA) sequence targeting Erbb4-IR (shRNA) at the age of 12, 15, and 18 weeks and sacrificed at 20 weeks. All mice were maintained in a standard animal house with a 12:12-h light/dark cycle and euthanized with an intraperitoneal injection of ketamine/xylene. The body weight was measured every 4 weeks. The renal cortexes were collected by carefully removing the renal pelvis and medullar tissues, which were used for real-time PCR and Western blot analysis or fixed in methyl Carnoy's for histological and immunohistochemical analysis. All studies were approval by the Animal Experimentation Ethics Committee, The Chinese University of Hong Kong, and the experimental methods were carried out in accordance with the approved guidelines.

Ultrasound-Mediated Gene Transfer Mediated Erbb4-IR Knockdown

A vector expressing Erbb4-IR–targeting shRNA (Erbb4-IR-shRNA-pSuper.puro) was constructed on shRNA-pSuper.puro vector with antisense sequence 5′-TCGAGGAATTCAAAAAAGCCTACAGTTTATCCACAATCTCTTGAATTGTGGATAAACTGTAGGCA-3′. Then, a noninvasive ultrasound-microbubble–mediated gene-transfer technique was used to deliver Erbb4-IR shRNA or empty pSuper.puro vector into both kidneys following the protocol as previously described (20). Briefly, mouse received the mixed solution (200 μL/mouse) containing either the Erbb4-IR shRNA or empty pSuper.puro vector and lipid microbubbles (Sonovue; Bracco, Milan, Italy) at a ratio of 1:1 (volume for volume) via the tail vein injection. Immediately after injection, an ultrasound transducer (Therasonic; Electro Medical Supplies, Wantage, U.K.) was directly placed on the skin of the back against the kidney with a pulse-wave output of 1 MHz at 2 W/cm^2 for a total of 5 min each side. To maintain the transgene expression levels, gene therapy was given at 12, 15, and 18 weeks. The experimental procedures were performed following the approved protocol by the Animal Experimentation Ethics Committee at The Chinese University of Hong Kong.

Cell Culture

To dissect the specific role and regulatory mechanisms through which TGF-β signals to Smad2 or Smad3 to regulate Erbb4-IR expression, characterized mouse embryonic fibroblasts (MEFs) lacking Smad3 or Smad2 were used for this study as described previously (22). AGE at a dose of 100 μg/mL (Sigma-Aldrich, St. Louis, MO) was added to induce responses. mTECs were cultured in DMEM/F12 (Gibco, Carlsbad, CA) supplemented with 5% FBS (Gibco) and 1% antibiotic/antimycotic solution (Life Technologies, Grand Island, NY). SV40-transformed mMCs (MES13; American Type Culture Collection, Manassas, VA) were maintained in a 3:1 mixture of DMEM and Ham's F-12 medium containing 5% FBS and 1% antibiotic/antimycotic solution (Life Technologies). Cells were cultured in 12- or 6-well plastic plates at 37°C in an incubator with 5% CO_2. Cells were stimulated with AGEs (100 μg/mL), normal glucose (5.5 mmol; Life Technologies), or high glucose (25 mmol; Life Technologies) for periods of 0, 1, 3, 6, 12, and 24 h in serum-free medium. BSA (100 μg/mL) or mannitol (25 mmol; Life Technologies) was used as NC.

Transient Small Interfering RNA–Mediated Silencing of Erbb4-IR

mTECs and mMCs were transfected with 100 nmol/L Erbb4-IR small interfering RNA (siRNA; sense 5′-GCCUACAGUUUAUCCACAAdTdT-3′ and antisense 3′-dTdTCGGAUGUCAAAUAGGUGUU-5′) or NC siRNA (sense 5′-AUGAACGUGAAUUGCUCAAUUU-3′ and antisense 3′-dTdTUACUUGCACUUAACGAGUUAAA-5′; RiboBio, Guangzhou, China) using Lipofectamine RNAiMAX reagent (Invitrogen, Carlsbad,

CA) according to the manufacturer's instruction (21). To examine the role of Erbb4-IR in diabetic renal fibrosis, mTECs and mMCs with or without Erbb4-IR siRNA were stimulated with AGEs (100 μg/mL) for 6 h. All cells were fasted with 0.5% FBS medium for 24 h before stimulation and maintained until the end of stimulation. Effects of downregulating Erbb4-IR on activation of TGF-β/Smad3 and expression of fibrotic markers (TGF-β1, phosphorylated [phospho]-Smad3, Smad3, collagen I, and collagen IV) were examined by real-time PCR or Western blot analysis.

Real-time PCR Analysis

Total RNA from renal cortex and cultured cells was isolated by TRIzol (Invitrogen) according to the manufacturer's instructions. Expression of mRNAs and miR-29b was measured by real-time PCR as previously described (23). The primers used in this study, including TGF-β1, collagen I, collagen IV, miR-29b, U6, and β-actin, were described previously (11). Other primers included: mouse Erbb4-IR forward 5′-AACTCGCCACAGAAATCCAC-3′ and reverse 5′-ACAACCCCAAACAAGCTGTC-3′. The relative level of detected gene was normalized with the internal control β-actin or U6 and expressed as mean ± SEM.

In Situ Hybridization

To detect the expression pattern and location of Erbb4-IR in the diabetic kidney, in situ hybridization was performed with double digoxigenin–labeled probes (Exiqon, Vedbæk, Denmark), following the protocol as described previously (20). Briefly, 10-μm slides were prepared from optimal cutting temperature compound–embedded kidney tissues. The slides were then fixed in 4% paraformaldehyde for 10 min and treated with proteinase-K (10 ng/mL) for 10 min at 37°C. Slides were prehybridized with the 1× ISH buffer (Exiqon) and then hybridized with digoxigenin antisense Erbb4-IR probes (5′-AATAGATATAACGACAATGTGT-3′) at 45°C for 1 h. After stringency washing, the sections were incubated with antidigoxigenin antibody (Roche Diagnostics, Indianapolis, IN) overnight at 4°C and developed with nitro blue tetrazolium/5-bromo-4-chloro-3-indolyl phosphate to produce positive signals. A scramble probe (5′-GTGTAACACGTCTATACGCCCA-3′) was used as an NC for all studies.

Fluorescence In Situ Hybridization and Immunofluorescence Assay

To detect the expression location of Erbb4-IR in the diabetic kidney and AGE-stimulated mTECs, in situ hybridization was performed with Cy3-conjugated Erbb4-IR probe (5′-AATAGATATAACGACAATGTGT-3′; GenePharma, Shanghai, P.R. China) or mouse U6 fluorescence in situ hybridization (FISH) probe (LNC110103; RiboBio) by using a FISH kit (C10910; RiboBio) according to the manufacturer's instruction. The kidney sections were further counterstained with FITC-conjugated epithelial cell marker keratins (Pan Cytokeratin antibody; 53-9003-82; eBioscience, San Diego, CA) by immunofluorescence assay as described in our previous study (24). The stained samples were imaged under fluorescence microscope (Axio Observer.Z1; Carl Zeiss, Oberkochen, Germany).

Western Blot Analysis

Protein from renal cortex and cultured cells was extracted using the radioimmunoprecipitation assay lysis buffer. Western blot analysis was performed as described previously (25). In brief, after blocking nonspecific binding with 5% BSA, nitrocellulose membranes were then incubated overnight at 4°C with primary antibodies against phospho-Smad3 (Cell Signaling Technology, Danvers, MA) and Smad3 (Santa Cruz Biotechnology, Santa Cruz, CA), collagens I and collagen IV (Southern Biotechnology Associates, Birmingham, AL), and β-actin (Santa Cruz Biotechnology), followed by IRDye800-conjugated secondary antibodies (Rockland Immunochemicals, Gilbertsville, PA). Signals were detected using the Li-Cor/Odyssey infrared image system (LI-COR Biosciences, Lincoln, NE), followed by quantitative analysis using the ImageJ program (National Institutes of Health; http://imagej.nih.gov/ij/). The ratio for the protein examined was normalized against β-actin and expressed as the mean ± SEM.

Fasting Blood Glucose, Intraperitoneal Glucose Tolerance Test, and Intraperitoneal Insulin Tolerance Test

Blood glucose levels were measured by AccuChek glucose meter (Roche Diagnostics) after the mouse fasting for 6 h every 4 weeks as recommended by the Animal Models of Diabetic Complications Consortium. Intraperitoneal glucose tolerance tests (IPGTTs) and intraperitoneal insulin tolerance tests (IPITTs) were performed at 20 weeks before sacrifice (26). Briefly, for IPGTT, mice were fasted for 6 h, D-glucose (1 mg glucose/gram body wt) was given intraperitoneally, and blood glucose levels were measured at 0, 15, 30, 60, and 120 min post–glucose challenge. For the IPITT, after a 3-h fast, mice received an intraperitoneal administration of 1 U/kg insulin, blood glucose levels were measured at 0, 15, 30, 60, and 120 min, and area under the curve was calculated.

Renal Function Measurement

The 24-h urinary samples were collected in metabolic cages every 4 weeks. Urinary microalbumin was measured by competitive ELISA according to the manufacturer's instructions (Exocell Inc, Philadelphia, PA). Urinary and serum creatinine were measured with an enzymatic kit (Stanbio Laboratories, Boerne, TX). Urinary albumin excretion was expressed as total urinary albumin/creatinine (in micrograms per milligram) as previously described (26).

Histology and Immunohistochemistry

Changes in renal morphology were examined in methyl Carnoy's fixed, paraffin-embedded tissue sections (4 μm) stained with the periodic acid-Schiff method. Immunostaining was performed in 4-μm paraffin sections using a microwave-based antigen retrieval technique (26). The antibodies used in this study included: collagen I and

collagen IV (Southern Biotechnology Associates) and phospho-Smad3 (Cell Signaling Technology). After immunostaining, sections were counterstained with hematoxylin (except for phospho-Smad3).

Quantitation of immunostaining was carried on coded slides as previously described (11). The expression of collagen I was quantified using Image-Pro Plus software (Media Cybernetics, Bethesda, MD) in 10 consecutive fields (original magnification ×200). The expression of collagen IV in the entire cortical tubulointerstitium (a cross-section of the kidney) was determined as previously described (26,27), whereas the expression in glomeruli was determined as described as follows: 20 glomeruli were randomly selected from each section, and positive signals within the selected glomerulus were highlighted, measured, and expressed as percentage positive area of the entire glomerulus. The numbers of phospho-Smad3 were counted in 20 consecutive glomeruli and expressed as cells per glomerular cross-section, whereas positive cells in the tubulointerstitium were counted under high-power fields (original magnification ×400) by means of a 0.0625-mm^2 graticule fitted in the eyepiece of the microscope and expressed as cells per millimeters squared.

Dual-Luciferase Reporter Assay

The pcDNA3.1$^+$ plasmid overexpressing Erbb4-IR full-length sequence (Erbb4-IR) and pGL3-basic reporter plasmid containing full-length miR-29b gene with (pGL3-miR-29b) or without 3′ untranslated region (UTR) sequence of predicted Erbb4-IR binding site (pGL3-mutant) (Supplementary Fig. 9) were constructed by BiOWiSH Technologies Ltd. (Beijing, China) (20). The luciferase reporter assay was performed by Landbiology (Guangzhou, China) by using a dual-luciferase reporter assay kit (Promega, Madison, WI), as in our previous studies (21,24). The empty (pGL3-basic) or miR-29b reporter plasmids (pGL3-miR-29b or pGL3-mutant) and Renilla-overexpressing plasmid (as internal control) were cotransfected into 293T cells with empty vector (pcDNA3.1$^+$) or Erbb4-IR–overexpressing plasmid (Erbb4-IR). Luciferase activities were measured at 48 h according to the manufacturer's instructions by the GloMax-Multi Detection System (Promega). The reporter activity was represented by the ratio of the firefly luciferase activity (M1) to the Renilla luciferase activity (M2) as M1/M2 and shown as mean ± SEM fold induction of luciferase in three independent experiments.

Erbb4-IR Overexpression and miR-29b Mimic Transfection

The mTECs were transfected with 0.5 μg/mL empty vector (pcDNA3.1$^+$) or plasmid containing Erbb4-IR full-length RNA sequence (Erbb4-IR) with or without 50 nmol/L miR-29b mimic (5′-UAGCACCAUUUGAAAUCAGUGUU-3′), constructed by PharmaGene (Shanghai, China) using Lipofectamine 2000 (Invitrogen) according to the manufacturer's manual, and refreshed the culture medium after 4 h. Then the transfected cells were collected at 24 h (20).

Statistical Analysis

All data are expressed as means ± SEM. Statistical analyses were performed with one-way ANOVA, followed by Newman-Keuls multiple comparison from Prism 5.0 (GraphPad Software, San Diego, CA). A two-way ANOVA was used for disease parameters obtained from Smad3-WT and -KO mice. In addition, a repeated-analysis ANOVA was used for albumin excretion, body weight, fasting blood glucose (FBG), IPITT, and IPGTT analysis.

RESULTS

Erbb4-IR Is Smad3-Dependently Increased in Mice During T2DN Progression

We previously identified that Erbb4-IR is a Smad3-dependent lncRNA in a kidney fibrosis mouse model by RNA-sequencing and chromatin immunoprecipitation assay (19,21), suggesting that Erbb4-IR may serve as a direct Smad3 target gene during the progression of kidney disease. To determine whether Erbb4-IR is also Smad3-dependently expressed in the progression of T2DN, we first examined its expression profile in the kidney of Smad3-WT and Smad3-KO *db/db* mice. Interestingly, real-time PCR analysis revealed that Erbb4-IR was significantly upregulated in the diabetic kidney of Smad3-WT but not in Smad3-KO *db/db* mice at 12 weeks of age (Fig. 1*A*). In situ hybridization further revealed that Erbb4-IR was markedly upregulated in the glomerular cells, presumably mesangial cells, and tubular epithelial cells of the kidney in *db/db* mice compared with *db/m* mice (Fig. 1*B*). The Erbb4-IR expression was further confirmed by FISH assay with immunofluorescence costaining of epithelial cell marker keratins. Results shown in Fig. 1*C* clearly demonstrated that expression of Erbb4-IR was largely increased in the nucleus of mesangial and epithelial cells with tubular cytosolic expression pattern, whereas a trace amount of Erbb4-IR was detected in epithelial cells but absent in the glomerulus of the normal kidney from *db/m* mice.

Erbb4-IR Expression Is Tightly Regulated by the AGE/Smad3 Signaling Pathway

We next investigated the mechanisms of AGE signaling in Erbb4-IR expression. As shown in Fig. 1*D*, AGE caused a remarkable increase in Erbb4-IR on Smad2-WT and Smad3-WT MEF cells. Interestingly, the AGE-induced Erbb4-IR expression was regulated by Smad3 but not Smad2 because knockout of Smad3 completely prevented AGE-induced Erbb4-IR expression, whereas deletion of Smad2 did not alter high levels of Erbb4-IR in response to AGEs by MEFs (Fig. 1*D*). In addition, we also detected that addition of AGEs (100 μg/mL) but not high glucose (25 mmol) was capable of inducing expression of Erbb4-IR by mTECs and mMCs in a time- and dose-dependent manner, peaking at 3 h (Figs. 2*A* and *B*, 3*A* and *B*, and Supplementary Fig. 1), which was associated with a marked upregulation of collagen I and collagen IV (Supplementary Fig. 2). Furthermore, blocking of receptors for AGE significantly reduced AGE-induced Erbb4-IR expression

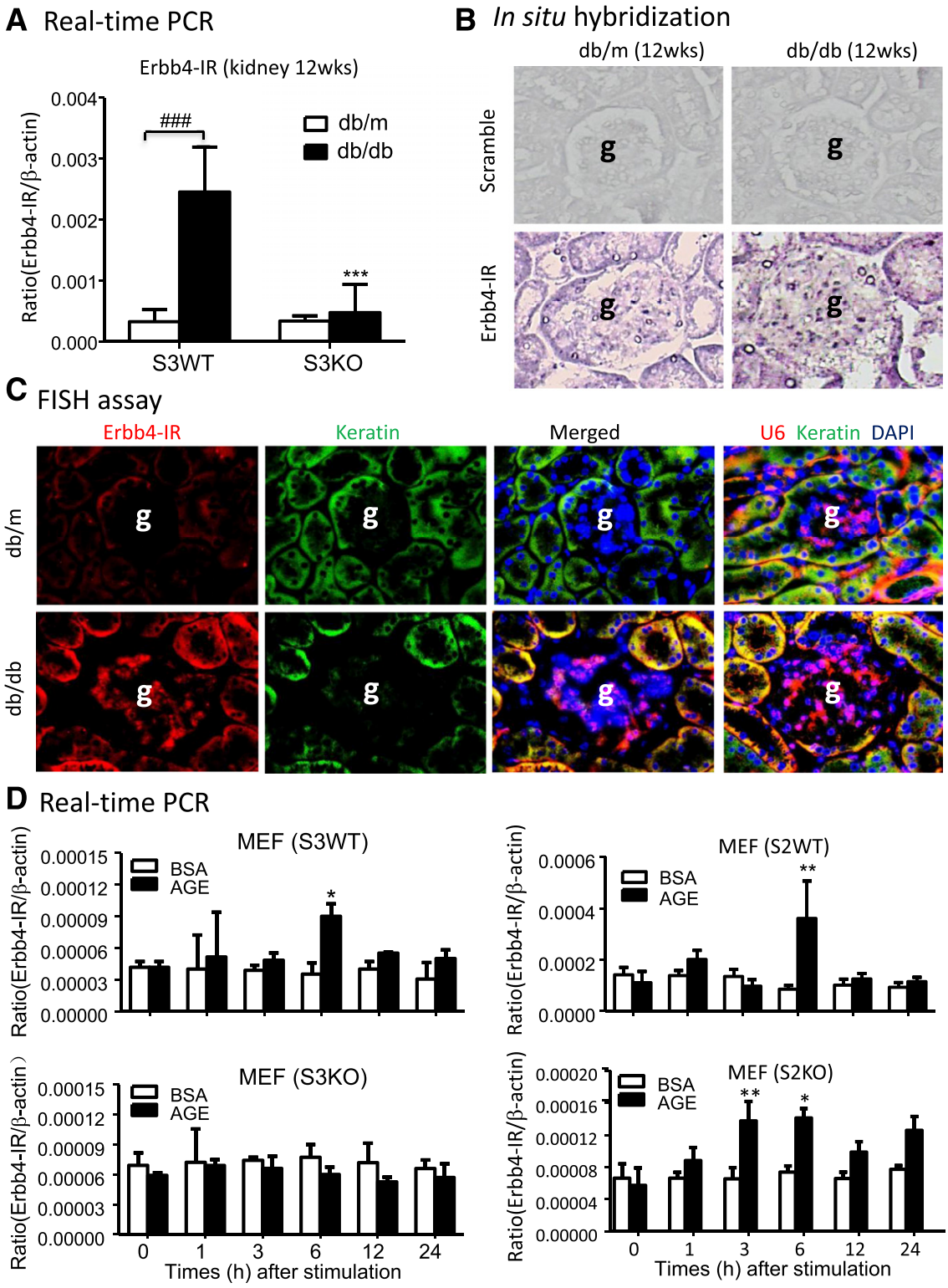

Figure 1—Erbb4-IR expression is upregulated in diabetic kidney and tightly regulated by TGF-β/Smad3 signaling. *A*: Real-time PCR detects that Erbb4-IR expression is largely increased in the kidney of Smad3-WT (S3WT) *db/db* mice, which is suppressed in the Smad3-KO (S3KO) *db/db* mice. *B*: In situ hybridization shows that Erbb4-IR is weakly expressed in the kidney of *db/m* mice. *C*: FISH assay with immunofluorescence costaining of epithelial cell marker keratins (green) further confirmed the upregulation of Erbb4-IR (red) was largely located at the nucleus (DAPI, blue) of glomerular mesangial cells and in perinuclear-cytoplasmic tubular epithelial cells of diabetic injured kidney in the *db/db* mice at week 12. U6 (red) is used as positive control, as shown in the right panel. *D*: Real-time PCR shows that addition of AGEs (100 μg/mL) induces Erbb4-IR expression in S3WT but not in S3KO MEF cells. However, its expression increases in both Smad2-WT (S2WT) and Smad2-KO (S2KO) MEF cells under AGE stimulation. Each bar represents the mean ± SEM for groups of six mice or three independent experiments. $^{*}P < 0.05$; $^{**}P < 0.01$; $^{***}P < 0.01$ vs. S3WT *db/db* or time 0; $^{\#\#\#}P < 0.001$ as indicated. Original magnification ×400 (*B* and *C*). g, glomerulus.

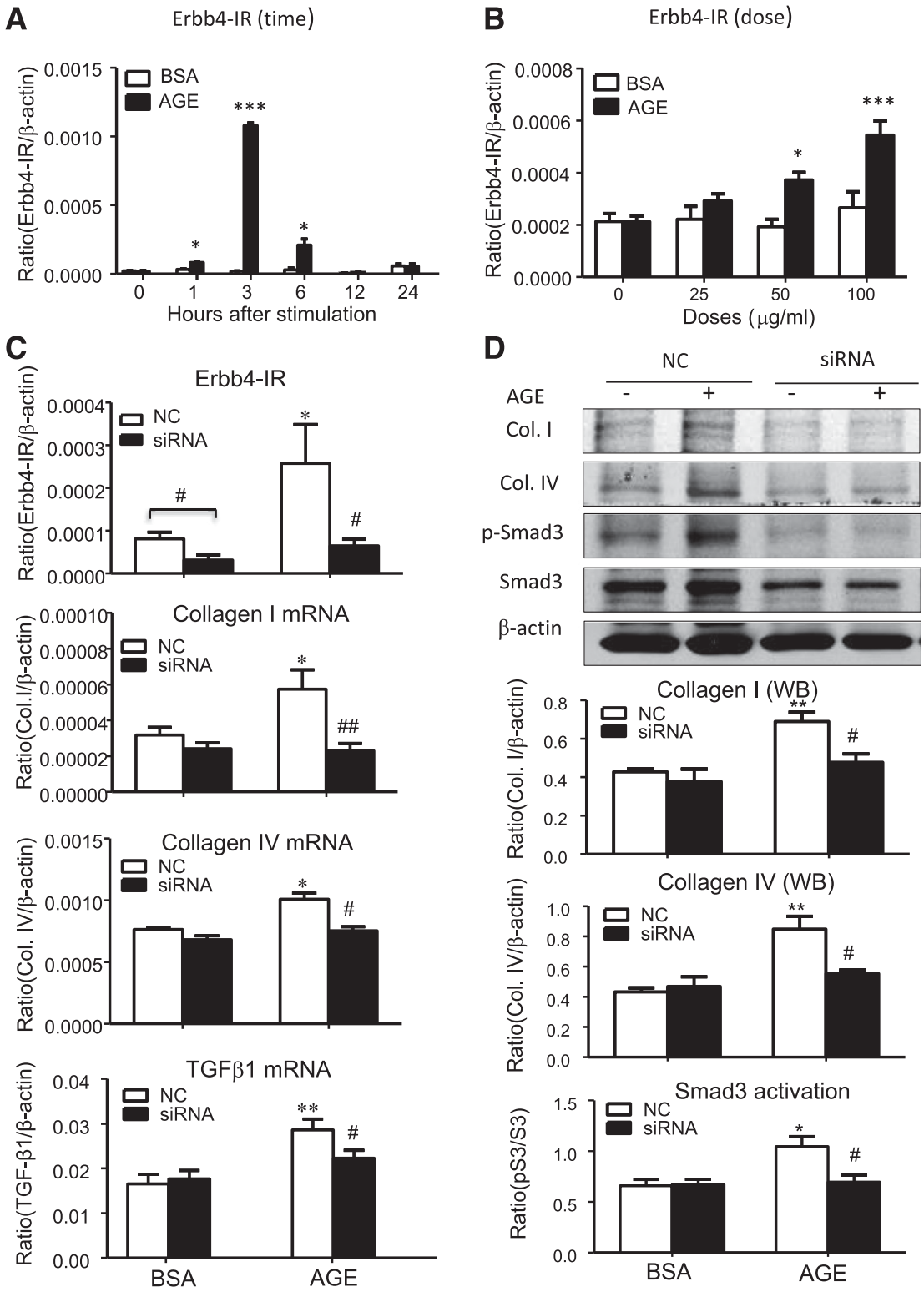

Figure 2—Knockdown of Erbb4-IR inhibits AGE-induced TGF-β1/Smad3-dependent fibrosis in mTECs. *A* and *B*: Real-time PCR shows that AGEs (100 μg/mL) induce Erbb4-IR expression in a time- and dosage-dependent manner, being significant at 1 h and peaking at 3 h with an optimal dose at 100 μg/mL. *C*: Real-time PCR detects that knockdown of Erbb4-IR inhibits AGE-induced (100 μg/mL) collagen I (Col. I), collagen IV (Col. IV), and TGF-β1 mRNA expression in mTECs. *D*: Western blot (WB) analysis shows that knockdown of Erbb4-IR decreases AGE-induced Col. I and Col. IV protein expression and inhibits phosphorylation of Smad3 (p-Smad3). Data represent the mean ± SEM for at least three independent experiments. *$P < 0.05$; **$P < 0.01$; ***$P < 0.001$ compared with the BSA control; #$P < 0.05$; ##$P < 0.01$ compared with NC with AGE stimulation. siRNA, Erbb4-IR siRNA.

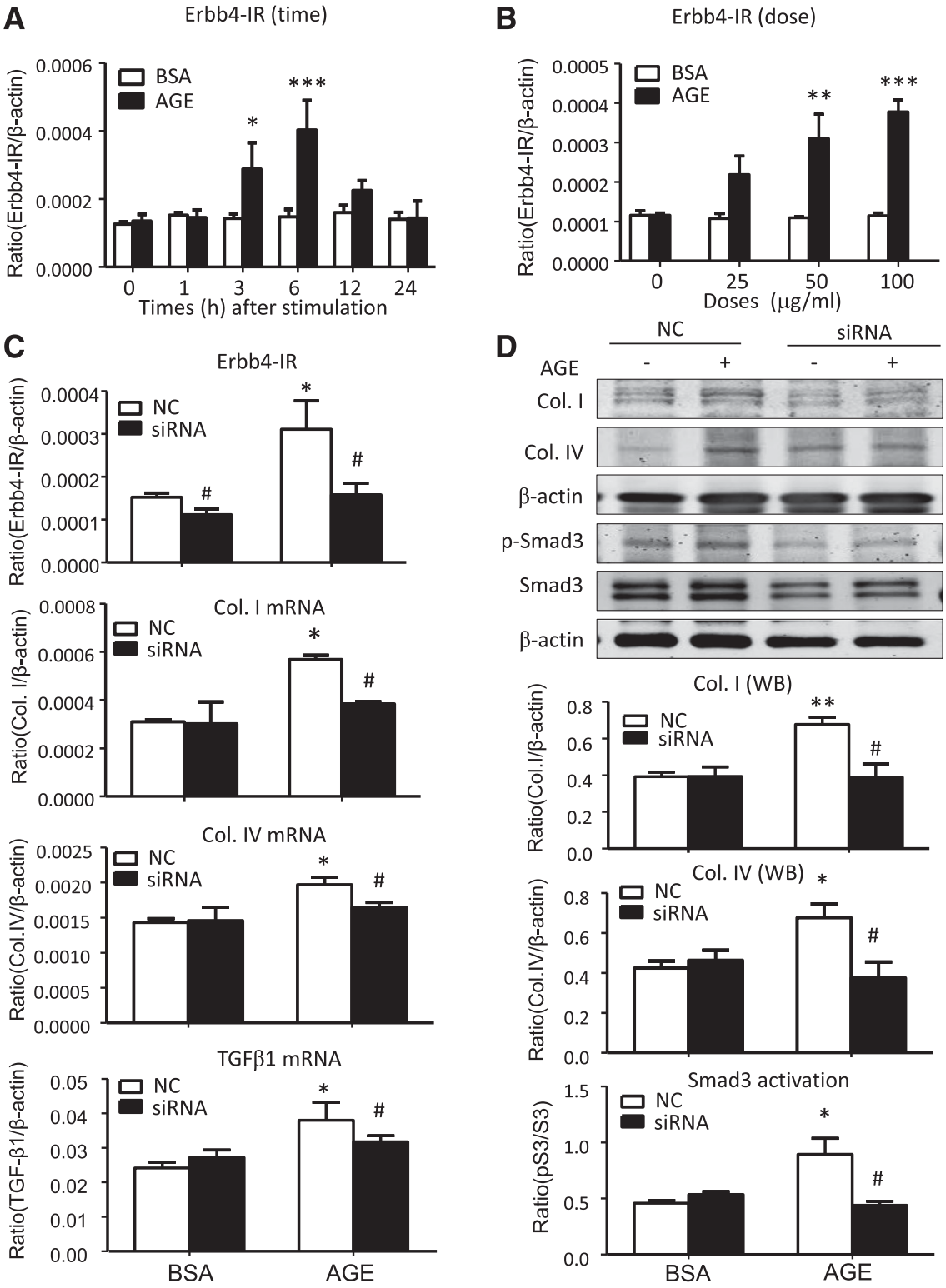

Figure 3—Knockdown of Erbb4-IR inhibits AGE-induced TGF-β1/Smad3-dependent fibrosis in mMCs. *A* and *B*: Real-time PCR shows that AGEs (100 μg/mL) induce Erbb4-IR expression in a time- and dosage-dependent manner, being significant at 3 h with an optimal dose at 100 μg/mL. *C*: Real-time PCR detects that knockdown of Erbb4-IR decreases AGE-induced (100 μg/mL) collagen I (Col. I), collagen IV (Col. IV), and TGF-β1 mRNA expression by mMCs. *D*: Western blot (WB) analysis shows that knockdown of Erbb4-IR decreases AGE-induced Col. I and Col. IV protein expression and inhibits phosphorylation of Smad3 (p-Smad3). Data represent the mean ± SEM for at least three independent experiments. *$P < 0.05$; **$P < 0.01$; ***$P < 0.001$ compared with BSA control; #$P < 0.05$ compared with NC with AGE stimulation. siRNA, Erbb4-IR siRNA.

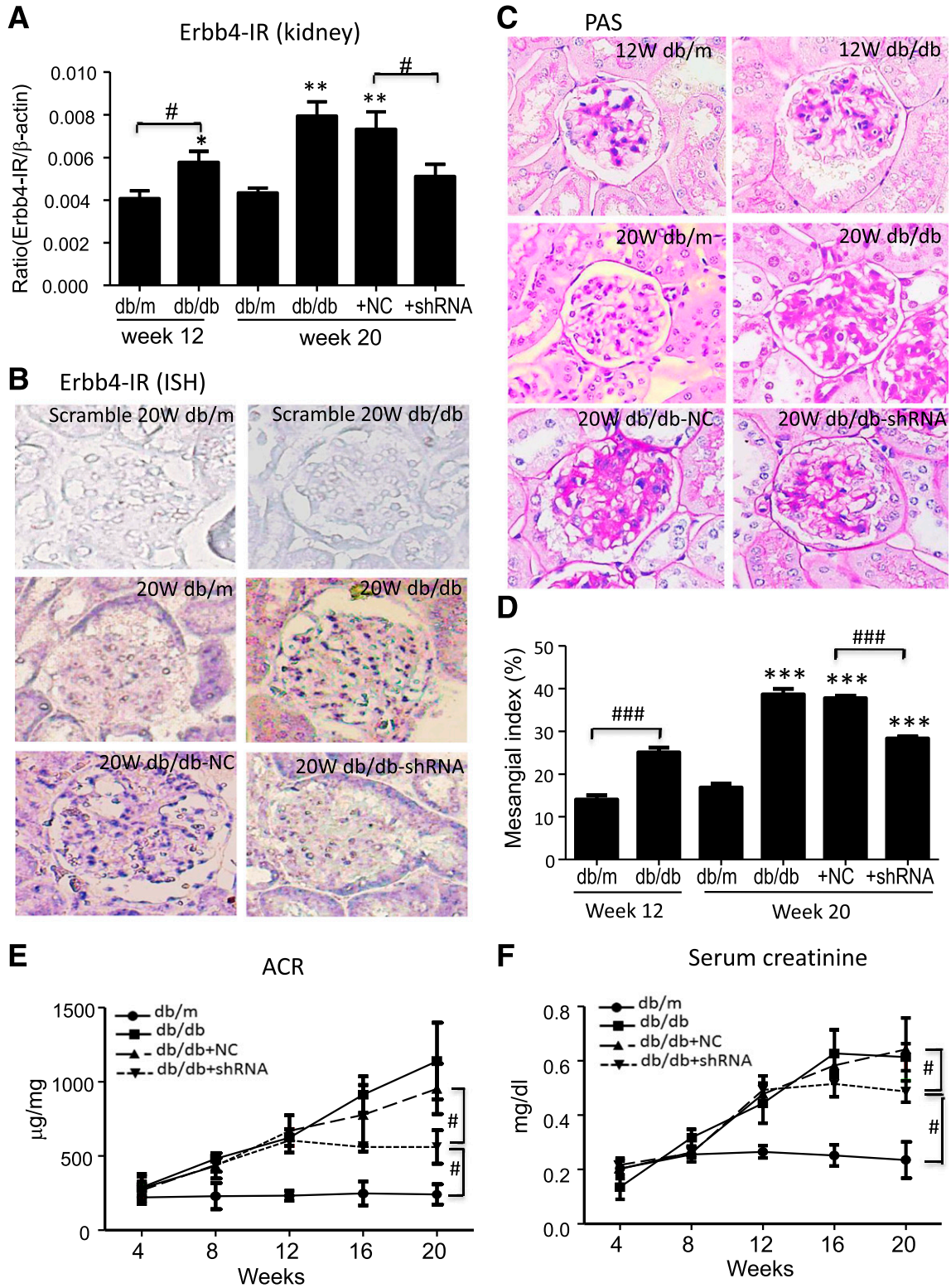

Figure 4—Effects of kidney-specific Erbb4-IR shRNA transfer on renal histology and functional injury in *db/db* mice. *A* and *B*: Real-time PCR and in situ hybridization (ISH) show that Erbb4-IR expression is significantly increased in the diabetic kidneys, presumably in mesangial cells and tubular epithelial cells, which is downregulated by Erbb4-IR gene therapy using the ultrasound-microbubble gene-transfer technique. Scramble probe is the NC for ISH. *C* and *D*: Knockdown of Erbb4-IR inhibits renal histological injury including mesangial matrix index by periodic acid-Schiff (PAS) staining. *E* and *F*: Knockdown of Erbb4-IR attenuates microalbuminuria creatinine ratio (ACR) and serum creatinine in *db/db* mice. Data represent the mean ± SEM for groups of six to eight mice. Original magnification ×400 (*B* and *C*). *$P < 0.05$; **$P < 0.01$; ***$P < 0.001$ vs. *db/m* mice; #$P < 0.05$; ###$P < 0.001$ as indicated. shRNA, *db/db* mice received Erbb4-IR shRNA treatment.

in mTECs (Supplementary Fig. 3). These results suggested that Erbb4-IR expression is tightly regulated by AGEs via a Smad3-dependent mechanism under diabetic conditions.

Knockdown of Erbb4-IR Attenuates AGE-Induced Fibrosis In Vitro

To study the functional role and potential mechanisms of Erbb4-IR in renal fibrosis, knockdown of Erbb4-IR was conducted on the mTECs and mMCs under AGE stimulation. Real-time PCR showed that siRNA-mediated knockdown significantly downregulated the expression of Erbb4-IR in both mTECs and mMCs (Supplementary Fig. 4). Furthermore, real-time PCR and Western blot analysis clearly demonstrated that silencing of Erbb4-IR significantly inhibited the fibrotic responses in the AGE-stimulated mTECs and mMCs, including expression of collagen I, collagen IV, TGF-β1, and phosphorylation of Smad3 (Figs. 2*C* and *D* and 3*C* and *D*).

Erbb4-IR Induction Is Associated With Activation of TGF-β/Smad3 Signaling and Progressive Renal Fibrosis in *db/db* Mice

We further examined whether Erbb4-IR expression is associated with the progression of T2DN in *db/db* mice. Real-time PCR and in situ hybridization showed that Erbb4-IR was significantly increased in *db/db* mice at the age of 12 to 20 weeks compared with the *db/m* mice (Fig. 4*A* and *B*). This was associated with the increase in mesangial matrix expansion (Fig. 4*C* and *D*), microalbuminuria creatinine ratio, serum creatinine (Fig. 4*E* and *F*), collagen I and IV expression (Figs. 5 and 6), as well as activation of TGF-β/Smad3 signaling (Fig. 7) in the *db/db* mice compared with the

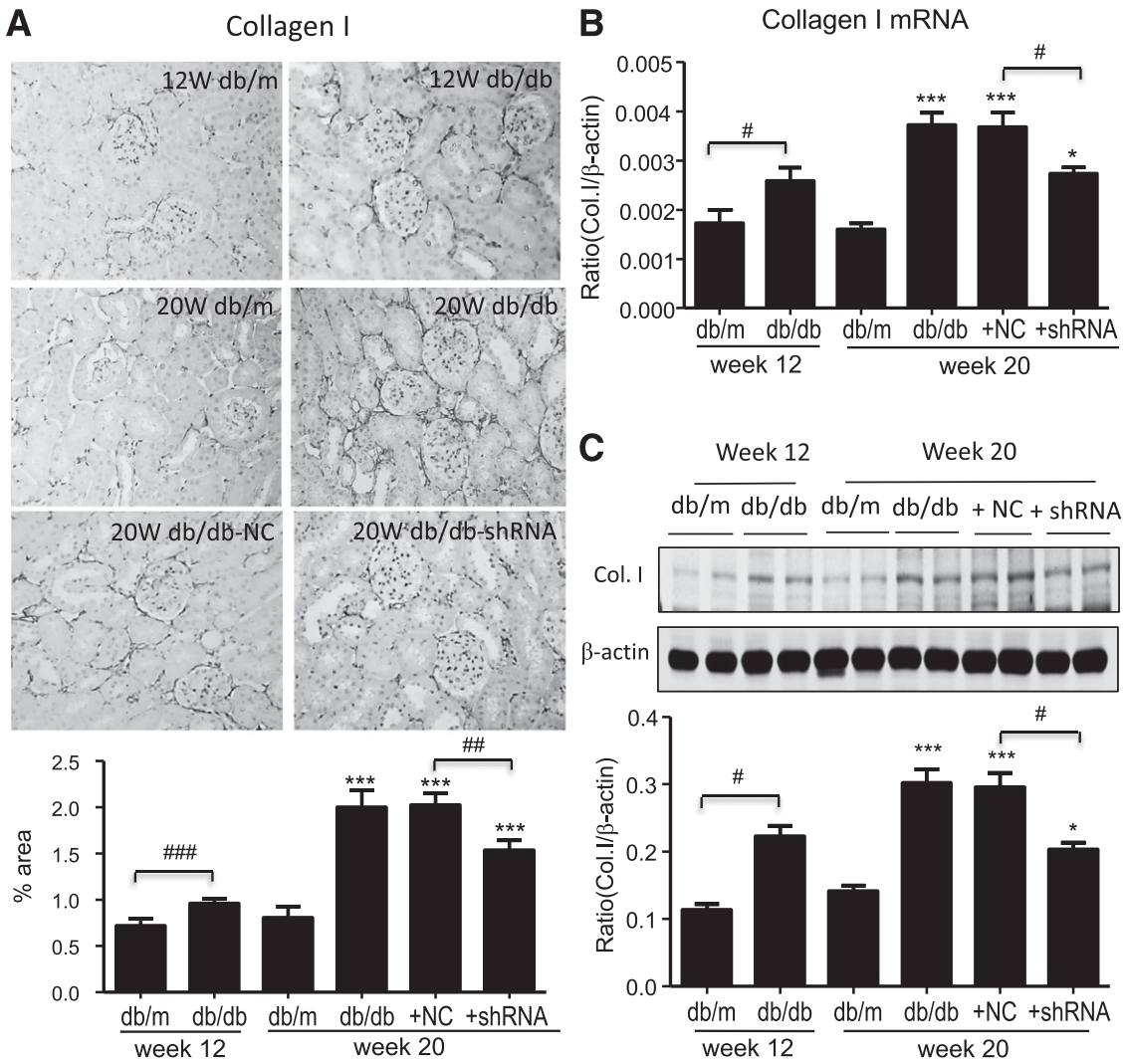

Figure 5—Knockdown of renal Erbb4-IR inhibits collagen I expression in the diabetic kidney of *db/db* mice. *A*: Immunohistochemistry and quantitative analysis of collagen expression. Original magnification ×200. *B*: Real-time PCR analysis of collagen I (Col. I) mRNA expression. *C*: Western blot analysis of collagen protein expression. Each bar represents the mean ± SEM for groups of six to eight mice. **P* < 0.05; ****P* < 0.001 compared with week 20 *db/m* mice; #*P* < 0.05; ##*P* < 0.01; ###*P* < 0.001 as indicated. NC, *db/db* mice received empty vector; shRNA, *db/db* mice received Erbb4-IR shRNA treatment.

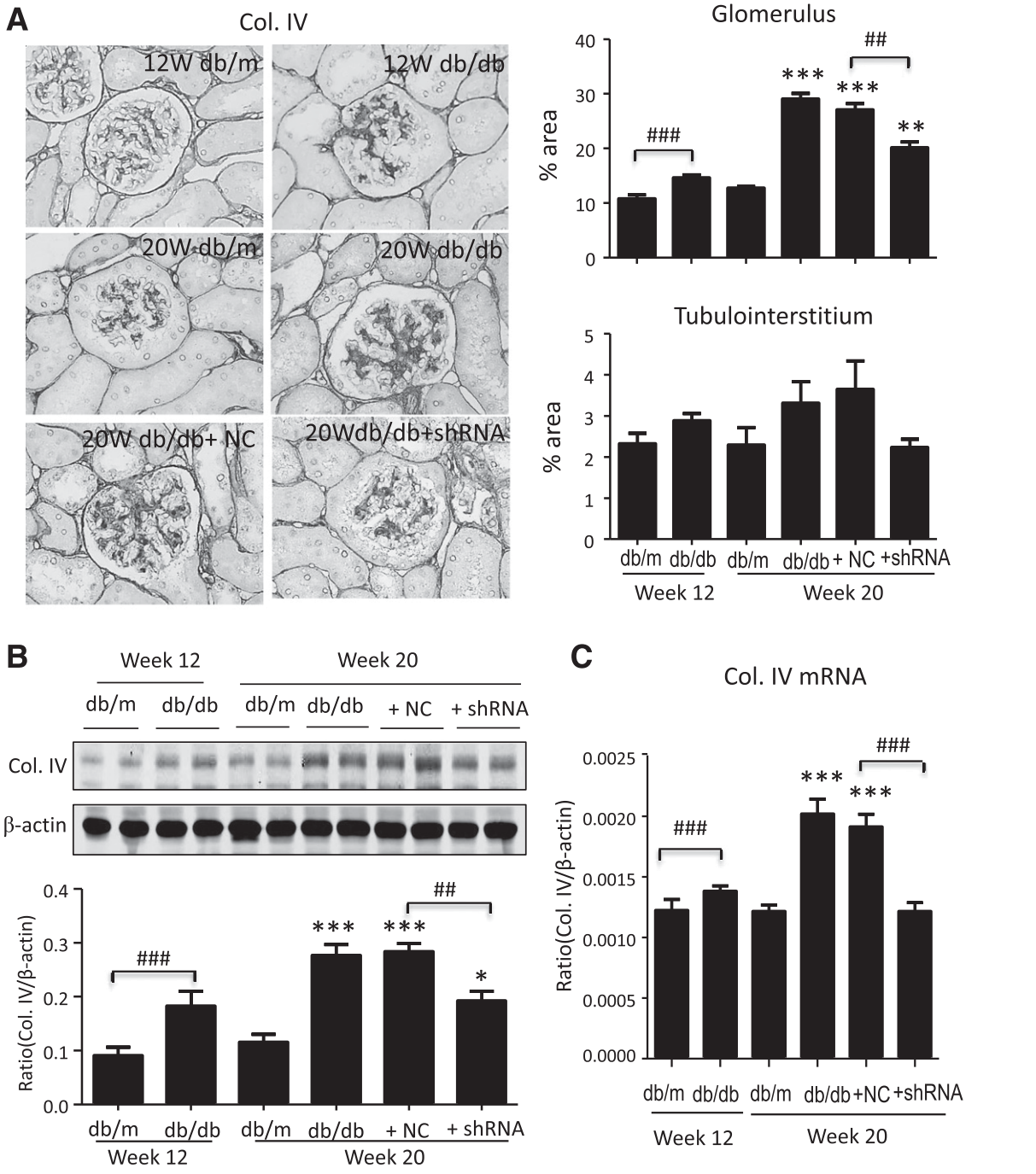

Figure 6—Knockdown of renal Erbb4-IR inhibits collagen IV (Col. IV) expression in the diabetic kidney of *db/db* mice. *A*: Immunohistochemistry and quantitative analysis of Col. IV expression. Original magnification ×400. *B*: Western blot analysis of Col. IV protein expression. *C*: Real-time PCR analysis of Col. IV mRNA expression. Each bar represents the mean ± SEM for groups of six to eight mice. *$P < 0.05$; **$P < 0.01$; ***$P < 0.001$ compared with week 20 *db/m* mice; ##$P < 0.01$; ###$P < 0.001$ as indicated. Col. I, collagen I; NC, *db/db* mice received empty vector; shRNA, *db/db* mice received Erbb4-IR shRNA treatment.

control group (*db/m* mice). Interestingly, the body weight and FBG were significantly increased in *db/db* mice since the age of 8 weeks compared with the *db/m* controls (Supplementary Fig. 5); these diabetic phenotypes occurred earlier than the induction of Erbb4-IR at week 12 (Supplementary Fig. 5), suggesting that Erbb4-IR may be involved in the development of kidney complications in diabetes.

Kidney-Specific Silencing of Erbb4-IR Inhibits Renal Injury in *db/db* Mice

We next examined the pathogenic role and therapeutic potential of Erbb4-IR in T2DN by using ultrasound-microbubble–mediated gene transfer of shRNA–Erbb4-IR plasmid. As shown in Fig. 4*A* and *B*, both real-time PCR and in situ hybridization detected that treatment with shRNA successfully

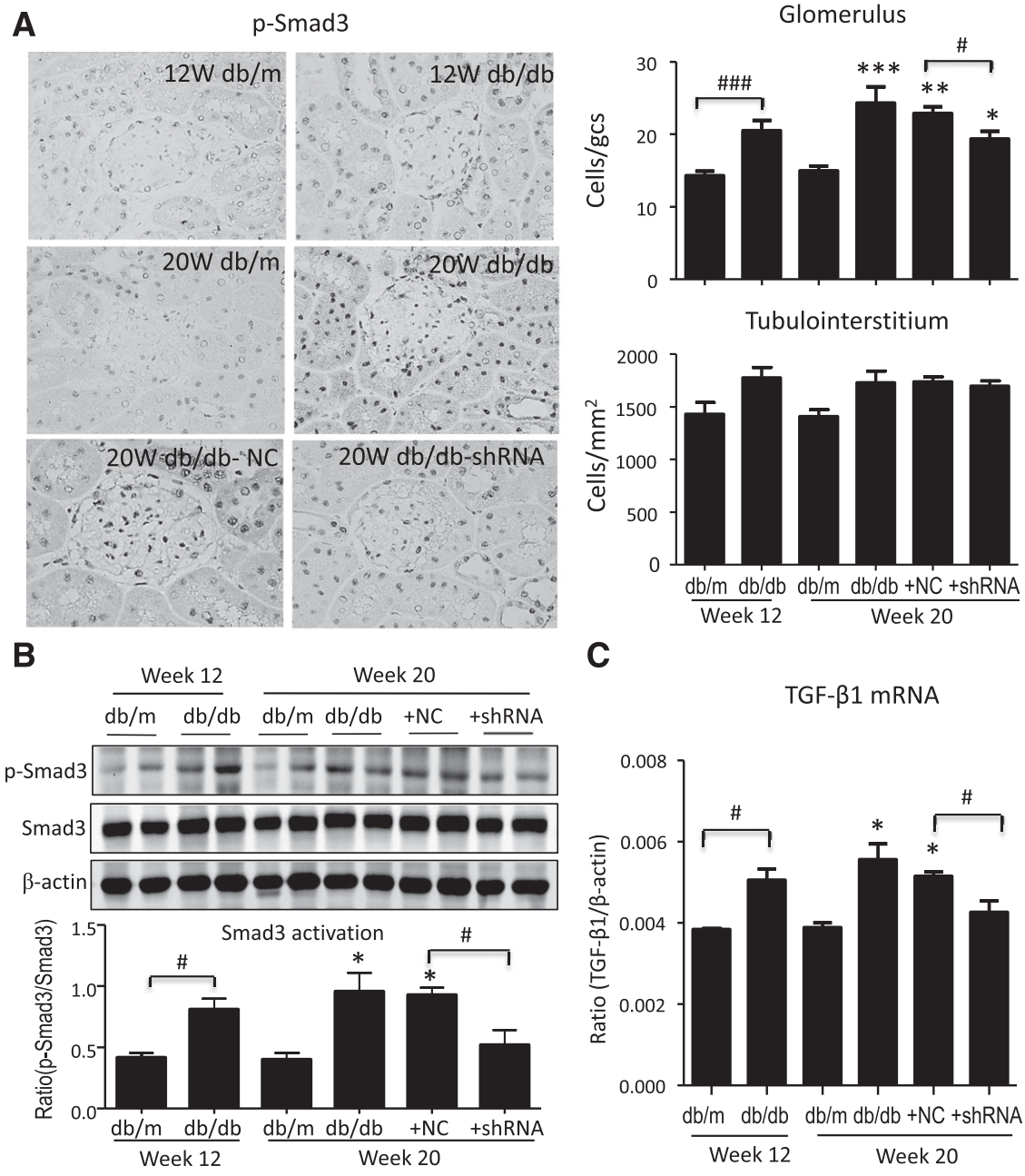

Figure 7—Knockdown of renal Erbb4-IR blocks activation of TGF-β/Smad3 signaling in the diabetic kidney of *db/db* mice. *A*: Immunohistochemistry and quantitative analysis for phosphorylation of Smad3 (p-Smad3) in glomerular and tubulointerstitial compartments. Original magnification ×400. *B*: Western blot analysis for phosphorylation of Smad3. *C*: Real-time PCR for TGF-β1 mRNA expression. Data show TGF-β1/Smad3 signaling activates from week 12. Contrarily, Erbb4-IR shRNA treatment inhibits the activation of signaling. Each bar represents the mean ± SEM for groups of six to eight mice. *$P < 0.05$; **$P < 0.01$; ***$P < 0.001$ compared with week 20 *db/m* mice; #$P < 0.05$; ###$P < 0.001$ as indicated. NC, *db/db* mice received negative control treatment; shRNA, *db/db* mice received Erbb4-IR shRNA treatment.

suppressed the expression of renal Erbb4-IR in *db/db* mice at the age of >12 to 20 weeks. More importantly, inhibition of renal Erbb4-IR expression largely improved renal histological injury (Fig. 4*C* and *D*) and decreased microalbuminuria excretion and serum creatinine (Fig. 4*E* and *F*). However, blockade of renal Erbb4-IR showed no effect on the syndromes of type 2 diabetes including body weight, FBG, IPGTT, and IPITT (Supplementary Fig. 6), suggesting a kidney-specific mechanism of Erbb4-IR in the development of T2DN.

miR-29b Is a Target of Erbb4-IR, and Blockade of Erbb4-IR Increases miR-29b to Protect Against Diabetic Kidney Injury in *db/db* Mice

Renal fibrosis is a hallmark of DN and is TGF-β/Smad3 dependent (28). We thus further elucidated whether the profibrotic effects of Erbb4-IR are established via the TGF-β/Smad3 signaling. As shown in Figs. 5 and 6, immunohistochemistry, real-time PCR analysis, and Western blot analysis demonstrated that both the mRNA and protein

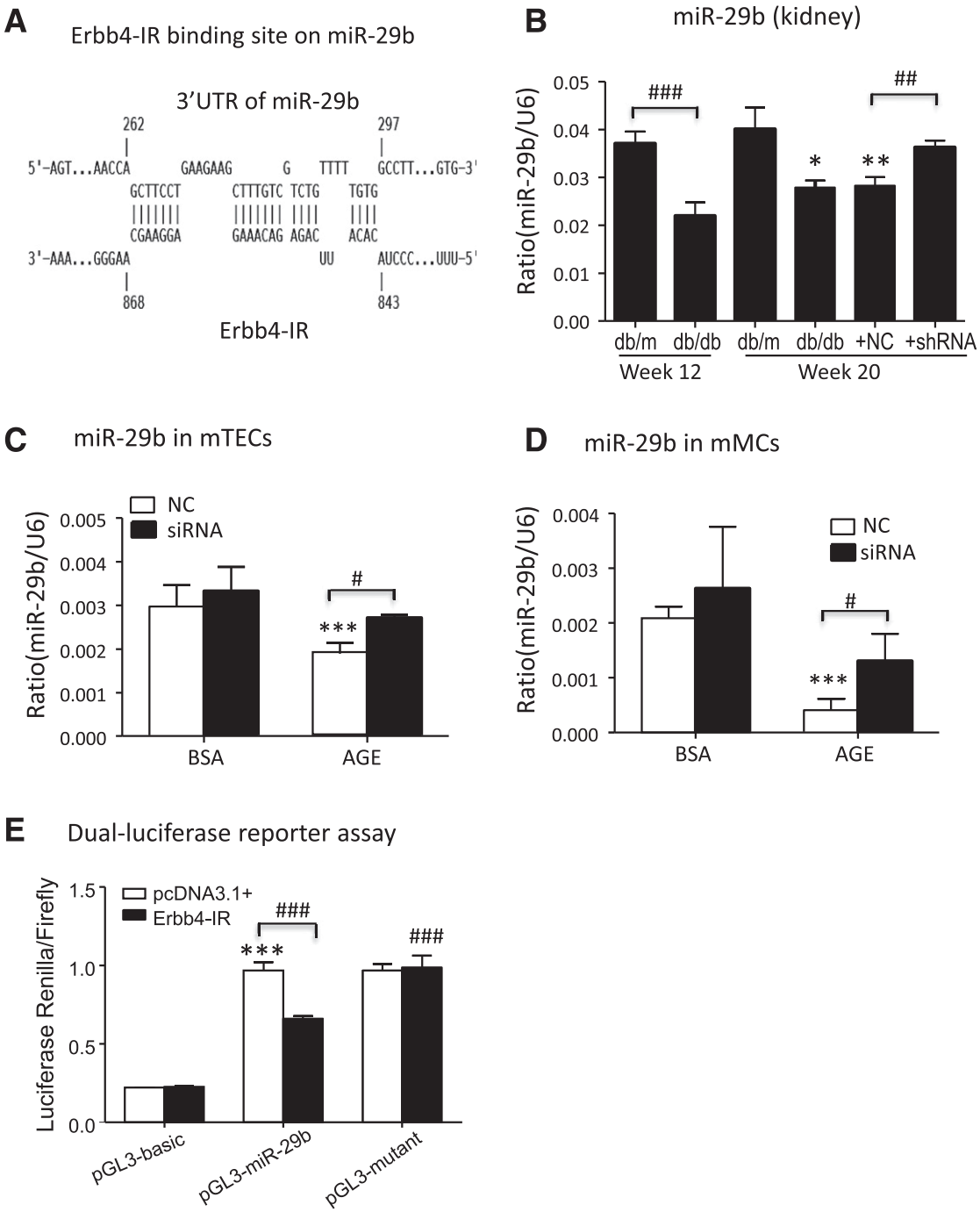

Figure 8—Erbb4-IR inhibits the expression of miR-29b at the transcriptional level. *A*: Predicted binding site of Erbb4-IR on the genomic sequence of miR-29b. *B*: Real-time PCR for expression of miR-29b in diabetic kidney. $^{*}P < 0.05$; $^{**}P < 0.01$ compared with week 20 *db/m* mice; $^{\#\#}P < 0.01$; $^{\#\#\#}P < 0.001$ as indicated. *C* and *D*: Real-time PCR for expression of miR-29b in mTEC and mMCs in response to AGE (100 μg/mL) stimulation at 3 h. $^{***}P < 0.001$ compared with NC with BSA control; $^{\#}P < 0.05$ as indicated. *E*: Dual-luciferase reporter assay shows that overexpression of Erbb4-IR largely inhibits the reporter activity of miR-29b compared with the empty vector control (pcDNA3.1^{+}), whereas the inhibitory effect was blocked by the deletion of predicted binding site of Erbb4-IR (pGL3-mutant). Each bar represents the mean ± SEM for groups of six to eight mice. $^{***}P < 0.001$ compared with empty vector (pcDNA3.1^{+}) with pGL3-basic; $^{\#\#\#}P < 0.001$ compared with Erbb4-IR overexpression (Erbb4-IR) with pGL3-miR-29b reporter plasmid as indicated.

expression levels of collagen I and IV were significantly suppressed by the kidney-specific knockdown of Erbb4-IR in *db/db* mice. Nevertheless, blockade of renal fibrosis by Erbb4-IR knockdown was largely attributed to the inhibition of TGF-β1 expression and phosphorylation of Smad3 in *db/db* mice (Fig. 7), revealing the pathogenic role of Erbb4-IR in TGF-β/Smad3-dependent renal fibrosis of DN.

Mechanistically, we found that AEG stimulation clearly increased Erbb4-IR level in the nuclear of mTECs in vitro, and a potential binding site of Erbb4-IR is predicted on the 3′ UTR of miR-29b genomic sequence (Fig. 8*A* and Supplementary Figs. 7 and 8). It has been well established that renal protective miR-29b is involved in the progression of TGF-β/Smad-dependent renal fibrosis under diabetic and nondiabetic conditions (11,29). To detect the interaction of Erbb4-IR and miR-29b, we measured the miR-29b expression in vivo and in vitro. Real-time PCR showed that renal miR-29b was largely decreased in *db/db* mice from the age of 12 to 20 weeks; but was significantly upregulated by the silencing of renal Erbb4-IR in vivo (Fig. 8*B*). Furthermore, consistent responses were also observed in vitro that addition of AGEs decreased the expression of miR-29b in mTEC and mMCs that were significantly reversed by the siRNA-mediated knockdown of Erbb4-IR (Fig. 8*C* and *D*). More importantly, transfection of miR-29b mimic significantly suppressed collagen I induction in mTECs with Erbb4-IR overexpression in vitro (Supplementary Fig. 9). Finally, the direct interaction between Erbb4-IR and 3′ UTR of miR-29b genomic sequence was confirmed by dual-luciferase reporter assay, in which overexpression of full-length Erbb4-IR dramatically inhibits the miR-29b transcription shown by the significant reduction in reporter activity (pGL3-miR-29b), which was blocked by the deletion of predicted Erbb4-IR binding site at the 3′ UTR miR-29b genomic sequence (pGL3-mutant), suggesting the inhibitory effect of Erbb4-IR on miR-29b expression at the transcriptional level (Fig. 8*E*).

DISCUSSION

In this study, we revealed a pathogenic role of lncRNA Erbb4-IR in T2DN and elucidated its molecular mechanism by using a novel T2DN mouse stain in Smad3-KO *db/db* mice. Our findings suggested that Erbb4-IR is a Smad3-dependent profibrotic lncRNA that directly inhibits the transcription of renoprotective miR-29b, therefore largely promoting renal fibrosis and renal dysfunction during the progression of T2DN. Thus, Erbb4-IR may represent a precise therapeutic target for T2DN.

The lncRNAs are defined as RNAs of >200 nucleotides without protein coding (30). Recently, perturbation of lncRNAs expression has begun to provide some insights into lncRNA function (31). However, the role of lncRNAs in kidney disease is still largely unknown (17,18,32,33). In our previous studies, we identified Erbb4-IR is a Smad3-associated lncRNA related to kidney injury by RNA sequencing (20). We found that the sequence of Erbb4-IR is partially conserved among species including human, it is a novel lncRNA independent of its host gene Erbb4 (21). However, its potential function in T2DN is still unexplored. In the present work, we revealed that Erbb4-IR is markedly upregulated in T2DN in Smad3-WT *db/db* mice, but largely suppressed in Smad3-KO *db/db* mice. In vitro, we also revealed that Erbb4-IR was specifically induced by AGEs but not by high glucose via the Smad3-dependent mechanism because deletion of Smad3 but not Smad2 blocked AGE-induced Erbb4-IR expression. More importantly, we demonstrated that silencing of Erbb4-IR largely inhibited TGF-β/Smad3-mediated renal fibrosis in vitro and in *db/db* mice. In contrast, Erbb4-IR shows no role in the glucose metabolism, as no significant changes in the FBG, insulin resistance, and glucose tolerance were detected in *db/db* mice received Erbb4-IR shRNA treatment. Thus, we identified that Erbb4-IR has a functional role in renal fibrosis under diabetic conditions and may represent a therapeutic target for diabetic kidney disease. Our findings clearly demonstrated the functional importance of lncRNAs in the pathogenesis of T2DN.

The role of TGF-β/Smad signaling pathway in DN has been clearly characterized by us and other researchers (14, 28). AGEs are able to induce renal fibrosis via the TGF-β/Smad-mediated fibrotic pathway, targeting Smad7 or Smad3, which may have therapeutic potential for DN (15). Based on these works, we have identified a number of Smad3-dependent miRNAs, such as let-7, antifibrotic miR-29, as well as profibrotic miR-21 and miR-433 (28). Previously, lncRNA was suggested as a competing endogenous RNA or a molecular sponge in modulating the expression and biological functions of miRNAs (34,35). In the current study, we identified the working mechanism of Erbb4-IR in T2DN. First, bioinformatics analysis showed that a physical binding site of Erbb4-IR is presented in the genomic sequence of miR-29b. Then we found that expression of miR-29b could be largely increased by the silencing of Erbb4-IR in vivo and in vitro. Furthermore, we demonstrated the physical interaction between Erbb4-IR and miR-29b 3′ UTR genomic sequence by dual-luciferase reporter assay. The renoprotective miR-29 directly targets the 3′ UTRs of collagen I and collagen IV, thereby suppressing renal fibrosis (36). Therefore, silencing of renal Erbb4-IR could repress the expression levels of collagen I and collagen IV by increasing transcription of miR-29b. In this study, we provided further evidence supporting the use of an noninvasive ultrasound-microbubble–mediated technique in kidney diseases. Targeting renal Erbb4-IR resulted in improved renal function and inhibited TGF-β/Smad3-mediated renal fibrosis in *db/db* mice.

In conclusion, our study proposed that Erbb4-IR is a Smad3-dependent profibrotic lncRNA, which promotes the progression of renal fibrosis in T2DN by suppressing miR-29b transcription. Our findings suggest that targeting Erbb4-IR may represent a novel and specific therapy for diabetic kidney disease.

Funding. This study was supported by grants from the Research Grants Council of Hong Kong (GRF 14117815 and T12-402/13N), Health and Medical Research Fund (HMRF 03140486), and the National Natural Science Foundation of China (8162010803).

Duality of Interest. No potential conflicts of interest relevant to this article were reported.

Author Contributions. S.F.S. conceived experiments, analyzed data, and drafted the article. P.M.K.T. designed and constructed plasmids; performed the reporter activity assay, FISH assay, Erbb4-IR overexpression, and miR-29b mimic in vitro assays; and edited the manuscript. M.F. carried out the in vitro study and

analyzed data. J.X. conducted in situ hybridization assay. X.R.H. generated the Smad3-KO *db/db* mice and conceived experiments of both animal models. R.C.W.M. and P.L. conceived the data analysis and discussion. H.Y.L. designed, supervised, and wrote the article.

Prior Presentation. Parts of this study were presented as an invited seminar lecture at the American Society of Nephrology Kidney Week, New Orleans, LA, 2 November 2017.

References

1. Skroblin P, Mayr M. "Going long": long non-coding RNAs as biomarkers. Circ Res 2014;115:607–609
2. Sheng SR, Wu JS, Tang YL, Liang XH. Long noncoding RNAs: emerging regulators of tumor angiogenesis. Future Oncol 2017;13:1551–1562
3. Liu B, Sun L, Liu Q, et al. A cytoplasmic NF-κB interacting long noncoding RNA blocks IκB phosphorylation and suppresses breast cancer metastasis. Cancer Cell 2015;27:370–381
4. Viereck J, Thum T. Circulating noncoding RNAs as biomarkers of cardiovascular disease and injury. Circ Res 2017;120:381–399
5. Thum T, Condorelli G. Long noncoding RNAs and microRNAs in cardiovascular pathophysiology. Circ Res 2015;116:751–762
6. Wu GC, Pan HF, Leng RX, et al. Emerging role of long noncoding RNAs in autoimmune diseases. Autoimmun Rev 2015;14:798–805
7. Arvaniti E, Moulos P, Vakrakou A, et al. Whole-transcriptome analysis of UUO mouse model of renal fibrosis reveals new molecular players in kidney diseases. Sci Rep 2016;6:26235
8. Zhou P, Chen Z, Zou Y, Wan X. Roles of non-coding RNAs in acute kidney injury. Kidney Blood Press Res 2016;41:757–769
9. Chung AC, Lan HY. MicroRNAs in renal fibrosis. Front Physiol 2015;6:50
10. Sharma K, Karl B, Mathew AV, et al. Metabolomics reveals signature of mitochondrial dysfunction in diabetic kidney disease. J Am Soc Nephrol 2013;24:1901–1912
11. Chen HY, Zhong X, Huang XR, et al. MicroRNA-29b inhibits diabetic nephropathy in db/db mice. Mol Ther 2014;22:842–853
12. Zhong X, Chung AC, Chen HY, et al. miR-21 is a key therapeutic target for renal injury in a mouse model of type 2 diabetes. Diabetologia 2013;56:663–674
13. Badal SS, Danesh FR. Diabetic nephropathy: emerging biomarkers for risk assessment. Diabetes 2015;64:3063–3065
14. Lan HY. Transforming growth factor-β/Smad signalling in diabetic nephropathy. Clin Exp Pharmacol Physiol 2012;39:731–738
15. Chung AC, Zhang H, Kong YZ, et al. Advanced glycation end-products induce tubular CTGF via TGF-beta-independent Smad3 signaling. J Am Soc Nephrol 2010;21:249–260
16. Li JH, Huang XR, Zhu HJ, et al. Advanced glycation end products activate Smad signaling via TGF-beta-dependent and independent mechanisms: implications for diabetic renal and vascular disease. FASEB J 2004;18:176–178
17. Kato M, Wang M, Chen Z, et al. An endoplasmic reticulum stress-regulated lncRNA hosting a microRNA megacluster induces early features of diabetic nephropathy. Nat Commun 2016;30:12864
18. Li SY, Susztak K. The long noncoding RNA Tug1 connects metabolic changes with kidney disease in podocytes. J Clin Invest 2016;126:4072–4075
19. Zhou Q, Chung AC, Huang XR, Dong Y, Yu X, Lan HY. Identification of novel long noncoding RNAs associated with TGF-β/Smad3-mediated renal inflammation and fibrosis by RNA sequencing. Am J Pathol 2014;184:409–417
20. Zhou Q, Huang XR, Yu J, Yu X, Lan HY. Long noncoding RNA Arid2-IR is a novel therapeutic target for renal inflammation. Mol Ther 2015;23:1034–1043
21. Feng M, Tang PM, Huang XR, et al. TGF-β mediates renal fibrosis via the Smad3-Erbb4-IR long noncoding RNA axis. Mol Ther 2018;26:148–161
22. Duan WJ, Yu X, Huang XR, Yu JW, Lan HY. Opposing roles for Smad2 and Smad3 in peritoneal fibrosis in vivo and in vitro. Am J Pathol 2014;184:2275–2284
23. Sun SF, Zhao TT, Zhang HJ, et al. Renoprotective effect of berberine on type 2 diabetic nephropathy in rats. Clin Exp Pharmacol Physiol 2015;42:662–670
24. Tang PM, Zhou S, Meng XM, et al. Smad3 promotes cancer progression by inhibiting E4BP4-mediated NK cell development. Nat Commun 2017;8:14677
25. Tang PM, Zhou S, Li CJ, et al. The proto-oncogene tyrosine protein kinase Src is essential for macrophage-myofibroblast transition during renal scarring. Kidney Int 2018;93:173–187
26. You YK, Huang XR, Chen HY, Lyu XF, Liu HF, Lan HY. C-reactive protein promotes diabetic kidney disease in db/db mice via the CD32b-Smad3-mTOR signaling pathway. Sci Rep 2016;6:26740
27. Zhao T, Sun S, Zhang H, et al. Therapeutic effects of Tangshen formula on diabetic nephropathy in rats. PLoS One 2016;11:e0147693
28. Meng XM, Nikolic-Paterson DJ, Lan HY. TGF-β: the master regulator of fibrosis. Nat Rev Nephrol 2016;12:325–338
29. Lorenzen JM, Thum T. Long noncoding RNAs in kidney and cardiovascular diseases. Nat Rev Nephrol 2016;12:360–373
30. Dykes IM, Emanueli C. Transcriptional and post-transcriptional gene regulation by long non-coding RNA. Genomics Proteomics Bioinformatics 2017;15:177–186
31. Li Y, Wang T, Li Y, et al. Identification of long-non coding RNA UCA1 as an oncogene in renal cell carcinoma. Mol Med Rep 2016;13:3326–3334
32. Zhou L, Xu DY, Sha WG, Shen L, Lu GY, Yin X. Long non-coding MIAT mediates high glucose-induced renal tubular epithelial injury. Biochem Biophys Res Commun 2015;468:726–732
33. Li X, Zeng L, Cao C, et al. Long noncoding RNA MALAT1 regulates renal tubular epithelial pyroptosis by modulated miR-23c targeting of ELAVL1 in diabetic nephropathy. Exp Cell Res 2017;350:327–335
34. Rashid F, Shah A, Shan G. Long non-coding RNAs in the cytoplasm. Genomics Proteomics Bioinformatics 2016;14:73–80
35. Long J, Wang Y, Wang W, Chang BH, Danesh FR. MicroRNA-29c is a signature microRNA under high glucose conditions that targets Sprouty homolog 1, and its in vivo knockdown prevents progression of diabetic nephropathy. J Biol Chem 2011;286:11837–11848
36. Xiao J, Meng XM, Huang XR, et al. miR-29 inhibits bleomycin-induced pulmonary fibrosis in mice. Mol Ther 2012;20:1251–1260